ARTICLES
PUBLISHED ONLINE: 8 NOVEMBER 2009 | DOI: 10.1038/NCHEM.433
nature chemistry

Identification of active Zr–WO_x clusters on a ZrO_2 support for solid acid catalysts

Wu Zhou[1], Elizabeth I. Ross-Medgaarden[2], William V. Knowles[3], Michael S. Wong[3], Israel E. Wachs[2] and Christopher J. Kiely[1]*

Tungstated zirconia is a robust solid acid catalyst for light alkane (C_4–C_8) isomerization. Several structural models for catalytically active sites have been proposed, but the topic remains controversial, partly because of the absence of direct structural imaging information on the various supported WO_x species. High-angle annular dark-field imaging of WO_3/ZrO_2 catalysts in an aberration-corrected analytical electron microscope allows, for the first time, direct imaging of the various species present. Comparison of the relative distribution of these WO_x species in materials showing low and high catalytic activities has allowed the deduction of the likely identity of the catalytic active site—namely, subnanometre Zr–WO_x clusters. This information has subsequently been used in the design of new catalysts, in which the activity of a poor catalyst has been increased by two orders of magnitude using a synthesis procedure that deliberately increases the number density of catalytically relevant active species.

Since the pioneering work of Hino and Arata, tungstated zirconia has received considerable attention as a strong solid acid catalyst for the isomerization of light (C_4–C_8) alkanes at low temperatures[1]. Although less active than sulfated zirconia catalysts[2], the enhanced thermal stability and resistance in hydrogen, oxygen and water atmospheres of WO_3/ZrO_2 materials offers an alternative catalyst for many practical industrial applications[1,3]. Over the past two decades, a variety of characterization techniques and catalytic performance testing studies have been applied to this system in an attempt to correlate structure with catalytic performance[4–13]. A number of surface species have been proposed to exist in this catalyst system at various WO_x loading levels, including surface mono-tungstate and poly-tungstate species, distorted WO_x clusters containing ZrO_x and well-ordered WO_3 nanocrystals[4–13]. However, the lack of clear direct imaging methods to definitively confirm or disprove the presence of the smallest WO_x surface species (that is, surface mono-tungstate, surface poly-tungstate and subnanometre WO_x distorted clusters) has hindered progress in elucidating which is responsible for the catalytic activity. Here, we report for the first time the application of aberration-corrected analytical electron microscopy to overcome this imaging difficulty and demonstrate that, among the multitude of WO_x species present in the WO_3/ZrO_2 catalyst system, the origin of catalytic activity is primarily associated with WO_x clusters that are ~0.8–1 nm in diameter and intermixed with a small amount of ZrO_x. We also demonstrate that knowledge of the key active species can be used in catalyst design and optimization. More specifically, we demonstrate that the activity of a poor catalyst can be improved by two orders of magnitude by using a new post-preparation procedure that deliberately increases the number density of the key catalytically active species.

A general consensus exists that catalytic performance depends strongly on the surface density of the WO_x species on the zirconia surface[3,5,7,8,11,13,14]. It has also been demonstrated that tungsten oxide supported on $ZrO_x(OH)_{4-2x}$ can have considerably greater acidity than model tungsten oxide catalysts in which the WO_x species are supported on well-defined ZrO_2 crystallites[1,13] (denoted hereafter as model $WZrO_2$-type materials). Ross-Medgaarden and colleagues[13] recently proposed a new model for the catalytically active site based on extensive studies of a series of supported $WO_3/ZrO_x(OH)_{4-2x}$ catalysts (denoted hereafter as WZrOH-type materials). These latter catalysts were synthesized by the aqueous impregnation of ammonium meta-tungstate onto an amorphous $ZrO_x(OH)_{4-2x}$ metastable support, followed by calcination in the 773–1,173 K temperature range. The surface density of the WO_x species is expressed as the number density of tungsten atoms on the catalyst surface (W atoms nm^{-2}), and is controlled by a combination of WO_x loading level and the calcination temperature used. Activities for all the catalyst samples were tested using the methanol dehydration reaction[15], and expressed in terms of turnover frequency (TOF, the number of methanol molecules converted per catalytic active site per second). For the WZrOH-type materials, it was found[13] in the low-surface-density range of WO_x (that is, <5 W atoms nm^{-2}, which corresponds to monolayer surface coverage) that these catalysts have a very low activity ($\sim 1 \times 10^{-2}$ s^{-1}); above monolayer coverage (>5 W atoms nm^{-2}) there is a 100-fold increase in catalytic activity, with a maximum at $\sim 7 \times 10^{-1}$ s^{-1}. The activity trend revealed by the methanol dehydration reaction[13] is similar to that obtained in the alkane isomerization and *n*-butanol dehydration reactions reported by other groups[3,5,7,8,14]. Based on compelling *in situ* Raman and UV–vis spectroscopy evidence and conventional transmission electron microscopy (TEM) studies, Ross-Medgaarden and colleagues[13] proposed that surface mono-tungstate and poly-tungstate species are the majority species present in low-activity catalysts having surface densities below monolayer coverage. The corresponding higher-activity catalysts, having loadings above monolayer coverage, also showed spectroscopic evidence of Zr-stabilized WO_x clusters (as opposed to pure crystalline WO_3 nanoparticles), which were postulated to be responsible for the enhanced catalytic performance[13].

Although there is general agreement that the highest catalytic activity is associated with intermediate WO_x surface densities (that is, 5–8 W atoms nm^{-2}), the detailed atomic-scale structure of

[1]Department of Materials Science and Engineering, Lehigh University, Bethlehem, Pennsylvania 18015, USA, [2]*Operando* Molecular Spectroscopy and Catalysis Laboratory, Department of Chemical Engineering, Lehigh University, Bethlehem, Pennsylvania 18015, USA, [3]Department of Chemical and Biomolecular Engineering, Rice University, Houston, Texas 77005, USA. *e-mail: chk5@lehigh.edu

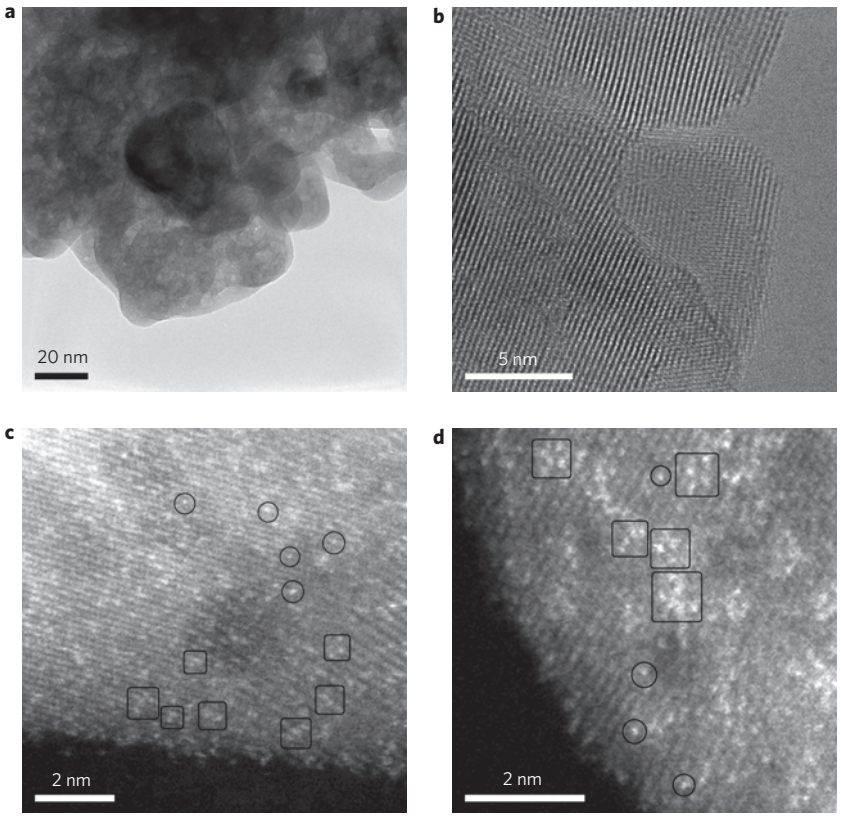

Figure 1 | Electron microscopy characterization of a low-activity WZrOH catalyst. a,**b**, Bright-field (**a**) and HRTEM micrographs (**b**) from a WZrOH sample that has a low catalytic activity (2.9WZrOH–773 K). **c**,**d**, HAADF images from the same sample in which the black circles highlight the presence of single tungsten atoms corresponding to surface mono-tungstate species and the black squares highlight surface poly-tungstate species with several tungsten atoms linked by oxygen bridging bonds.

the catalytic active site is still a controversial subject, several active site models having been proposed in the literature. Based on UV–vis diffuse reflectance spectroscopy, Raman spectroscopy and steady-state reaction studies, Iglesia and colleagues[5–7,16] assigned the active site structure to surface poly-tungstate species. Scheithauer and colleagues[4,14] favoured a fully oxidized poly-tungstate Keggin-like network structure incorporating trace levels of surface-exposed Zr^{4+} as the active species. Santiesteban and colleagues[3,17,18] postulated that a site having a 1:1 ratio of strong Brønsted-to-Lewis acid character would generate optimum catalytic performance, although a detailed structural model of the catalytic active site was not provided. The basic discrepancy between these various models revolves around whether the active sites are (i) a network of two-dimensional surface poly-tungstates or (ii) three-dimensional clusters of either pure WO_x or a mixed ZrO_x/WO_x species. To date, using high-resolution transmission electron microscopy (HRTEM) imaging techniques, it has not been possible to directly image, at the atomic scale, all of the possible WO_x species present, so the identity of the active site structure is still unresolved. We demonstrate here, for the first time, that atomic-resolution high-angle annular dark-field (HAADF) imaging[19,20] in a scanning transmission electron microscope (STEM) can generate high-contrast images and hence provide direct structural information on the type and distribution of tungsten oxide species present in the WO_3/ZrO_2 catalyst system.

Results and discussion

Aberration-corrected HAADF imaging on a 200 kV STEM[21], providing *Z*-contrast information with sub-ångström spatial resolution and single-atom sensitivity[20,22], was applied to investigate the subset of WZrOH catalysts discussed in ref. 13. Previously, this technique has been successfully applied to structural studies of supported metal catalysts such as La/Al_2O_3 (ref. 23), Au/TiO_2 (ref. 24) and Au/FeO_x (ref. 25), but little work has been done on supported metal oxide catalysts[26–28]. Low-contrast HAADF images are usually expected for oxides-on-oxides as a consequence of having (i) a very high dispersion of the overlayer oxide on the support and (ii) a relatively small *Z*-difference between the two components. Fortuitously for WO_3/ZrO_2, there is a large *Z*-difference and the various overlayer species are relatively stable and seem to retain their structural integrity under the electron beam during image acquisition, as demonstrated in Supplementary Fig. S1.

Figure 1a,b shows representative bright-field and HRTEM electron micrographs from a low-surface-density sample having low catalytic activity (2.9WZrOH–773K; TOF $= 1.4 \times 10^{-2}$ s^{-1}; see Methods for sample notation). Neither of these imaging modes shows any evidence of mono-tungstate, poly-tungstate, subnanometre WO_x clusters or discrete WO_3 nanocrystals on the nanocrystalline ZrO_2 support. In comparison, a highly dispersed array of bright flecks on the support, which correspond to individual tungsten atoms, can be clearly resolved using HAADF imaging (Fig. 1c,d). The fact that individual tungsten atoms are observed by *Z*-contrast now confirms that we are seeing all the WO_x species present. Although oxygen atoms are not resolved by HAADF imaging, all the tungsten species in this sample are known to be fully oxidized after the high-temperature calcination step because they show a characteristic W=O vibration at $\sim$1,020 cm^{-1} in Raman spectra[12,13]. Careful inspection of Fig. 1c,d reveals that there are actually two different types of tungsten arrangements present on the surface. Features highlighted by black circles correspond to isolated surface mono-tungstate species, each containing a single tungsten atom; those in black squares are indicative of surface poly-tungstate species having a two-dimensional network

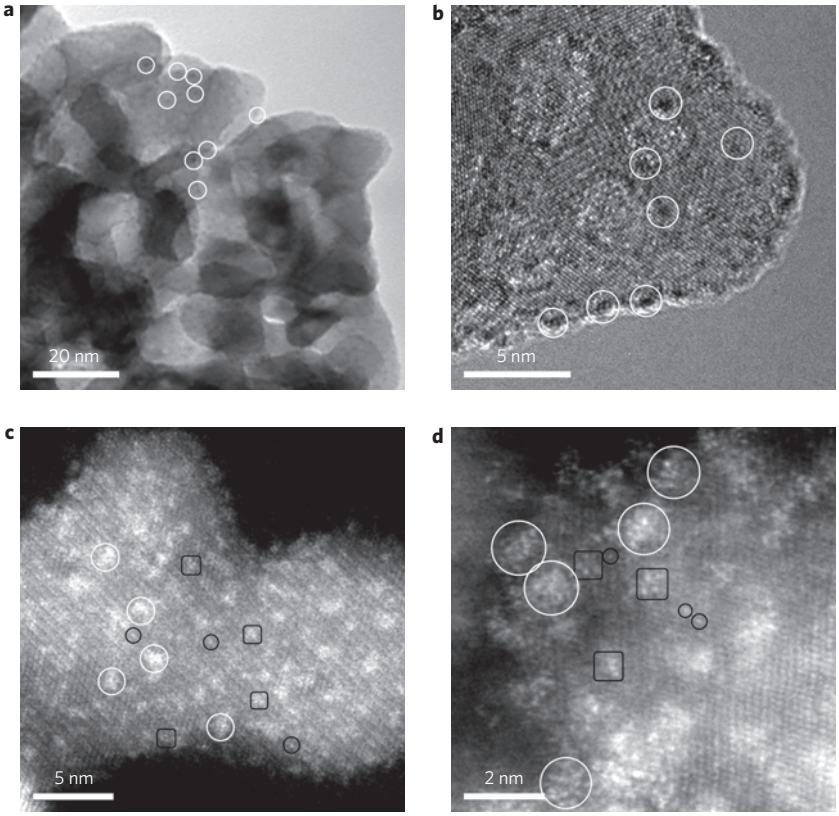

Figure 2 | Electron microscopy characterization of a high-activity WZrOH catalyst. a–d, Bright-field (**a**), HRTEM micrograph (**b**) and HAADF (**c**,**d**) images from a WZrOH sample with high catalytic activity (6.2WZrOH-1,073 K). Black circles indicate the presence of single tungsten atoms corresponding to surface mono-tungstate species. Black squares indicate surface poly-tungstate species with several tungsten atoms linked by oxygen bridging bonds. White circles indicate WO_x clusters with diameters of ~0.8–1.0 nm. These clusters were found only in samples with a surface density above monolayer coverage, which show higher catalytic performance.

structure with several tungsten atoms being linked via oxygen bridging bonds.

The projected W–W distances of the surface poly-tungstate species directly measured from multiple HAADF images show several characteristic separations (that is, 2.6 Å, 3.0 Å and 3.3 Å) that fall within the range of calculated W–W distances in $W_3O_n^-$ trimers (2.5–3.5 Å) (ref. 29). The slightly smaller experimental values may be due to the inclination of the ZrO_2 surface with respect to the incident electron beam and possible bond length contraction. Although the existence of surface mono-tungstate and poly-tungstate species has been proposed previously[6,7,12,13], this is the first time, to the best of our knowledge, that these entities have been directly visualized. The coexistence of surface poly-tungstate and mono-tungstate species at this low surface density (2.9 W atoms nm^{-2}) suggests that if a critical WO_x coverage is required for the formation of poly-tungstate species, it lies somewhere below 2.9 W atoms nm^{-2}, as was also similarly indicated by UV–vis spectroscopy[13] (1.7 W atoms nm^{-2}), as opposed to a coverage value of ~4.0 W atoms nm^{-2} as suggested previously[6,7]. The fact that tungsten atoms are preferentially located above zirconium columns, as observed in the HAADF images (Figs 1, 2, 4, 5 and Supplementary Fig. S2), suggests that strong bonding occurs between the ultra-dispersed WO_x species and the underlying surface hydroxyls of the ZrO_2 support. This observation is consistent with the characteristic Raman band at ~900–925 cm^{-1} observed for this type of sample, which has been assigned to bridging W–O–Zr bonds[13]. It is feasible that tungsten atoms may be preferentially associated with point defect sites on the ZrO_2 surface, a location that may also help stabilize the metastable tetragonal ZrO_2 polymorph often found in this catalyst system.

Figure 2a,b shows representative bright-field and HRTEM electron micrographs from a sample (6.2WZrOH–1,073 K) above monolayer WO_x coverage that shows high catalytic activity (TOF = 6.94×10^{-1} s^{-1}). As indicated, nanometre-scale dark flecks can just be discerned in these images, indicative of WO_x clusters. However, if one examines HAADF images (Fig. 2c,d), a clearer picture emerges in which surface mono- and poly-tungstate species coexist with numerous additional WO_x clusters that are 0.8–1 nm in diameter. These clusters exhibit higher contrast than the mono-tungstate and poly-tungstate species, suggesting that they are three-dimensional structures consisting of two or more atomic layers of WO_x. Determination of the precise number of tungsten atoms and their spatial configuration in these clusters is not possible because of their apparent disordered arrangement and the likelihood of variations in the W–O–W bond distances and angles[29]. Nevertheless, a rough estimate is still informative, and a 0.8–1 nm cluster would probably contain 10–15 WO_x units.

Simple correlation of the dramatic improvement in catalytic activity with the onset of WO_x cluster formation when monolayer coverage is exceeded implies that these cluster species are the most active sites in this catalyst. It has previously been proposed[5] that larger WO_x domains would be beneficial in dispersing the extra electron densities transferred onto the WO_x species during the catalytic reaction and, thus, help in stabilizing acidic sites in this system. Because these ~0.8–1 nm clusters contain significantly more WO_x structural units than the raft-like surface poly-tungstate species (which have 2–6 WO_x units) and isolated surface mono-tungstate species, it is not too surprising that they should show greater catalytic activity than the ultra-dispersed species.

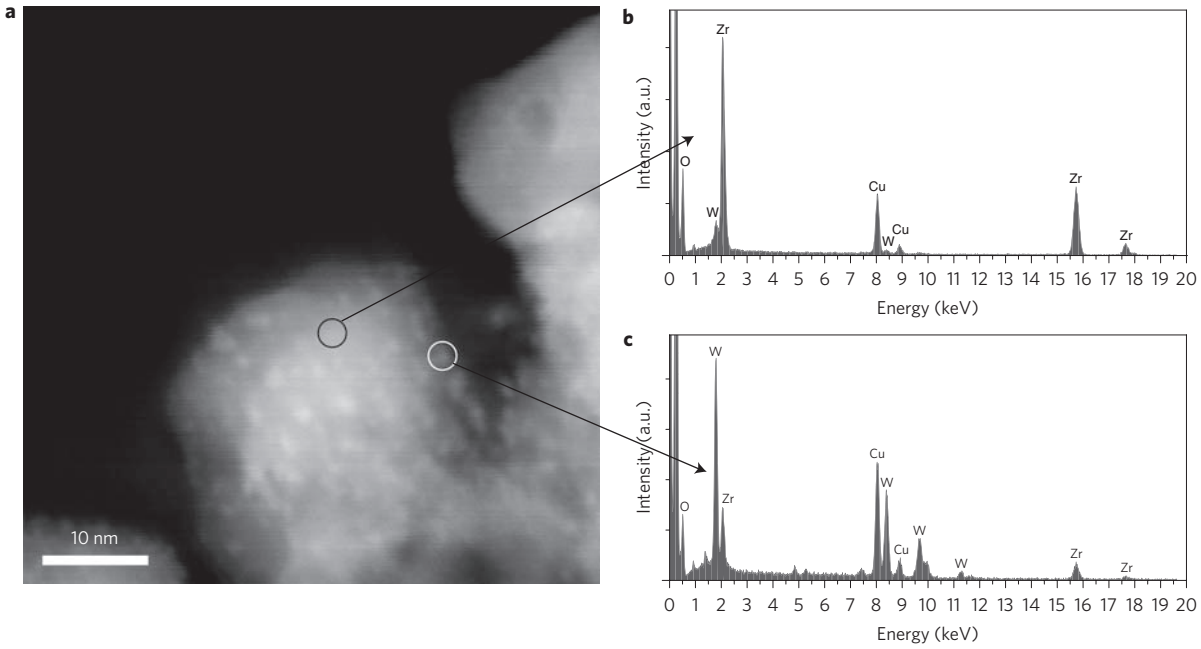

Figure 3 | STEM–XEDS analysis of a highly active WZrOH catalyst. a–c, XEDS chemical microanalysis on a ZrO_2 support and WO_x clusters from a highly active WZrOH catalyst having a WO_x surface density in excess of monolayer coverage: HAADF image (**a**); XEDS point spectrum from the ZrO_2 support-only area indicated by the black circle in **a** (**b**); XEDS point spectrum from a WO_x cluster near the edge of the ZrO_2 support particle, marked by a white circle in **a** (**c**). A very weak tungsten signal is observed in **b**, which may arise from surface mono- and poly-tungstate species that are not resolved in this low-resolution HAADF image. The cluster spectrum in **c** shows a significant enhancement in the tungsten signal, confirming that the cluster is tungsten rich. A weak zirconium signal is also observed in **c**, which arises from the underlying ZrO_2 support material and possibly any zirconium atoms that are incorporated within the cluster structure.

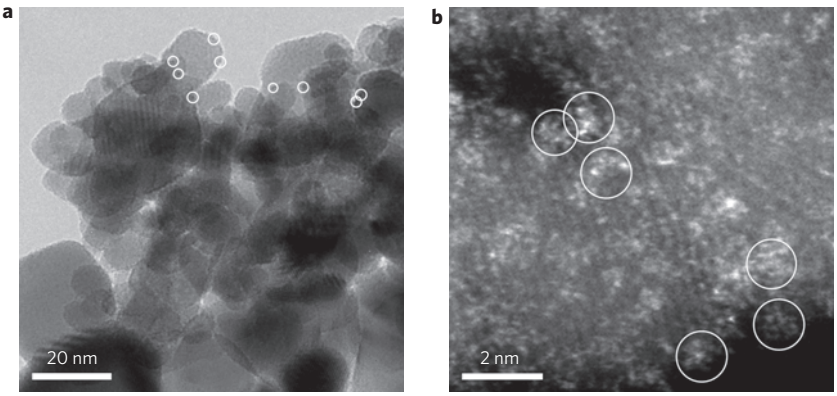

Figure 4 | Electron microscopy characterization of an inactive model $WZrO_2$ catalyst. a,**b**, Representative bright-field TEM (**a**) and HAADF (**b**) images from a model $WZrO_2$ catalyst calcined at 723 K (5.9$WZrO_2$–723 K) with a surface density greater than monolayer coverage. WO_x clusters ~0.8 nm in size are apparent (white circles). This sample was synthesized by impregnation of WO_x onto heat-treated crystalline Degussa ZrO_2 particles, and has very low catalytic activity.

To investigate the composition of these nanometre-scale clusters, X-ray energy dispersive spectroscopy (XEDS) analysis was performed using an aberration-corrected 300 kV VG HB603 STEM[30]. XEDS point analysis (Fig. 3) from a single cluster near the edge of a support particle suggests that the cationic component in the cluster is mainly tungsten. Previous *in situ* UV–vis spectra obtained from these samples indicate the presence of W^{6+} species, which can be partially reduced to W^{5+} during reactions[8,13]. However, neither XEDS analysis nor other optical spectroscopy results[13] can definitively address the question as to whether or not there are trace levels of ZrO_x intermixing within these WO_x clusters. The weak zirconium XEDS signal noted in Fig. 3c could be generated from the underlying ZrO_2 crystallite and any zirconium atoms incorporated within the cluster structure. Although, in principle, it should be possible to focus a sub-ångström electron beam 'edge-on' to a WO_x cluster in profile view on the ZrO_2 support, in order to perform high-sensitivity XEDS[30] or electron energy loss spectroscopy (EELS)[31], we are limited in this study by the instability of these subnanometre clusters under the prolonged high-energy electron illumination required for chemical analysis[32]. Moreover, it is impossible to prove the intermixing of ZrO_x and WO_x clusters using extended X-ray absorption fine structure (EXAFS)[33,34] or surface analysis techniques such as X-ray photoelectron spectroscopy (XPS) and low-energy ion scattering (LEIS) due to the ubiquitous presence of the ZrO_2 support and potential impurities within the ZrO_2 itself. However, neither can these techniques

Table 1 | Steady-state turnover frequency values for the methanol dehydration reaction for a systematic set of supported tungsten oxide catalyst samples.

Samples	Total tungsten surface density (W atoms nm^{-2})	Tungsten atoms nm^{-2} added	Zirconium atoms nm^{-2} added	Activity (normalized)
2.5WZrO$_2$-723 K	2.5	0	0	1*
(3.5W + 3.5Zr)/2.5WZrO$_2$-973 K	6.0	3.5	3.5	167
(3.5W)/2.5WZrO$_2$-973 K	6.0	3.5	0	4.8
(3.5Zr)/2.5WZrO$_2$-973 K	2.5	0	3.5	1.7
6.2WZrOH-973 K†	6.2	NA‡	NA	118
5.9WZrO$_2$-723 K	5.9	NA	NA	2.6

*Turnover frequency, TOF = 1.2 × 10^{-3} s^{-1}.
†Adapted from ref. 13.
‡NA, not applicable.

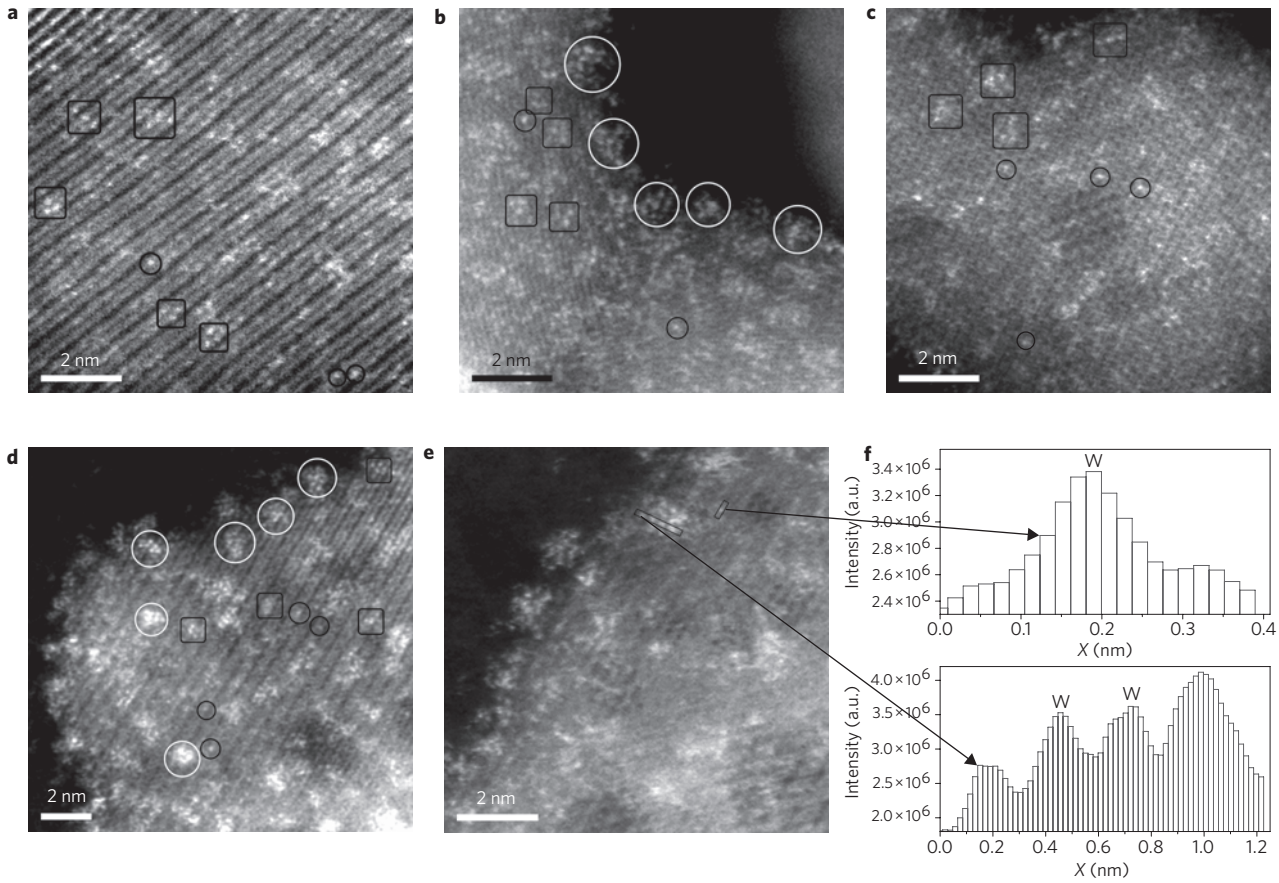

Figure 5 | STEM-HAADF imaging of post-impregnated catalysts. a–e, Aberration-corrected HAADF images of the starting low-surface-density model catalyst (2.5WZrO$_2$-723 K) (**a**); the post-impregnation catalyst with additional WO$_x$ only ((3.5W)/2.5WZrO$_2$-973 K) (**b**); the post-impregnation catalyst with additional ZrO$_x$ only ((3.5Zr)/2.5WZrO$_2$-973 K) (**c**); the highly active co-impregnation catalyst ((3.5W + 3.5Zr)/2.5WZrO$_2$-973 K) (**d**,**e**). Black squares indicate surface poly-tungstate species with several tungsten atoms linked by oxygen bridging bonds. White circles indicate WO$_x$ clusters with diameters of ~0.8–1.0 nm. **f**, Line intensity profile from a single tungsten atom and across a WO$_x$ cluster as indicated in **e**.

rule out the possibility of Zr–WO$_x$ intermixing. In fact, the ZrO$_2$–WO$_3$ phase diagram indicates the existence of bulk WZr oxide compounds[35].

The catalysts described so far were synthesized by the impregnation of ammonium meta-tungstate onto an amorphous ZrO$_x$(OH)$_{4-2x}$ support, so it is plausible that mixed Zr/W oxide clusters may be formed during the calcination step. From HAADF imaging, some subtle contrast variations are indeed noticeable within each cluster, hinting that occasional cation positions inside the clusters may actually be occupied by zirconium atoms. For comparative purposes, a model WZrO$_2$ catalyst (5.9WZrO$_2$–723 K) was synthesized by impregnation of the ammonium meta-tungstate precursor onto the model crystalline ZrO$_2$ support, followed by calcination at 723 K. When imaged in HAADF mode (Fig. 4) subnanometre size WO$_x$ clusters were found in this WZrO$_2$-type material having a nominal WO$_x$ coverage greater than a monolayer. However, the activity of this model WZrO$_2$ catalyst (TOF = 3.1 × 10^{-3} s^{-1}) is two orders of magnitude lower than the comparable WZrOH catalyst, suggesting that the active clusters in the latter catalyst have a different composition (that is, mixed Zr–WO$_x$). This is a reasonable expectation because it should be easier to extract and incorporate zirconium cations from the metastable decomposing ZrO$_x$(OH)$_{4-2x}$ than a stable pre-formed ZrO$_2$ crystallite during calcination.

On the basis of the HAADF and catalysis data presented so far, there is strong circumstantial evidence, but not direct definitive proof, that the most active sites in the WO_3/ZrO_2 catalysts are supported subnanometre, three-dimensional WO_x clusters that contain some zirconium cations. To test this hypothesis further, a catalyst design experiment was devised in which a relatively inactive $WZrO_2$ catalyst below monolayer coverage ($2.5WZrO_2$–723 K) was post-impregnated with (i) ZrO_x or WO_x precursors, separately, or (ii) both precursors, simultaneously, followed by a 973 K calcination step. Simultaneous co-impregnation with both WO_x and ZrO_x precursors is expected to mimic the formation of mixed-oxide clusters on the surface. The catalytic performances of the starting $WZrO_2$ catalyst and its various post-impregnated variants are summarized in Table 1. The activity of the catalyst co-impregnated with both ZrO_x and WO_x precursors simultaneously increases by two orders of magnitude relative to the model $WZrO_2$ base material. The new activity value attained is comparable with that of the most active WZrOH-type materials. In contrast, post-impregnation with the ZrO_x precursor or WO_x precursor alone shows only a minimal improvement in catalytic performance.

The starting low-activity $WZrO_2$ model catalyst (Fig. 5a) exclusively shows highly dispersed surface mono- and poly-tungstate species as expected, making this material an ideal platform for post-impregnation experiments. After subsequent impregnation of more WO_x precursor material, followed by calcination, an more population of 0.8–1 nm WO_x clusters was created (Fig. 5b). As the calcination temperature used (973 K) is well below the 1,494 K Tammann temperature of ZrO_2, it is unlikely that zirconium species will diffuse from the bulk ZrO_2 crystal into the surface WO_x clusters. Post-impregnation with ZrO_x alone results in a catalyst displaying only surface mono- and poly-tungstate species (Fig. 5c); no clusters were formed and the apparent WO_x surface coverage was comparable with that of the starting material. The additional ZrO_x material could presumably just epitaxially template onto the exposed ZrO_2 support. Alternatively, the additional Zr^{4+} cations could become inserted into the pre-existing surface polytungstate networks, as suggested by Santiesteban and colleagues[3,17,18]. If this were occurring, it does not result in enhanced catalytic activity. The sample co-impregnated with ZrO_x and WO_x shows an additional high-density population of subnanometre oxide clusters, presumably this time containing both tungsten and zirconium cations (Fig. 5d,e). Because the calcination temperature is comparable to the 896 K Hüttig temperature of ZrO_2 (in which surface species have sufficient mobility to agglomerate and sinter), there is a good chance of the surface WO_x and ZrO_x species becoming intermixed and incorporated into the clusters. It is also interesting to note that HAADF intensity variations can exist within the latter cluster type, as is evident from line intensity profiles (Fig. 5e,f). The centre of the cluster indicated shows an intensity level similar to that of a nearby isolated tungsten atom, whereas an atom at the periphery of the cluster shows obviously lower intensity. Although intensity variations in HAADF images can be caused by several factors[36], the variation noted here could, in principle, originate from the successful inclusion of a zirconium atom within this particular WO_x cluster.

These post-impregnation experiments clearly demonstrate that both ZrO_x and WO_x in an intimately mixed form are crucial in forming the catalytically active sites. Our postulate that the 0.8–1 nm mixed Zr–WO_x clusters constitute the most catalytically active species in the WO_3/ZrO_2 catalyst system has also been verified indirectly. The precise role of the small amount of incorporated ZrO_x species is still unknown, but first-principles calculations[37] informed by our electron microscopy observations are planned to determine the relationship between the electronic structure and catalytic performance of these mixed oxide clusters. Further understanding of the structure/performance relationship could, in principle, help us design even better catalysts by controlling the Zr–W ratio or replacing ZrO_x with other species.

Conclusions

HAADF imaging in an aberration-corrected STEM has been used to investigate the nanoscale structures present in supported WO_3/ZrO_2 solid acid catalysts. For the first time, we provide direct atomic-scale imaging of all the supported WO_x species present, including surface mono- and poly-tungstate species and subnanometre clusters. By correlating structural observations with catalytic activity measurements, we propose that 0.8–1 nm WO_x clusters incorporating some zirconium cations are the most active species in this catalyst system. When it becomes feasible to perform aberration-corrected HAADF imaging experiments within an environmental cell microscope, it would be fascinating to verify this proposal under reaction conditions. Co-impregnation of WO_x and ZrO_x precursors onto a pre-existing low-activity model $WZrO_2$ catalyst confirmed the importance of intimately mixed WO_x and ZrO_x entities within the clusters. This work also provides a clear demonstration of the principle that if the active species in a heterogeneous catalyst system can be positively identified, appropriate modifications to the catalyst preparation route can be devised to increase the number density of these desirable species, and hence improve the overall activity of the catalyst. Finally, in Supplementary Fig. S3 we demonstrate that this imaging technique has more general applicability to other supported oxide-on-oxide catalyst systems.

Methods

Catalyst preparation. *Preparation of $WO_3/ZrO_x(OH)_{4-2x}$ (denoted WZrOH catalysts).* Tungstated zirconia catalysts having various weight percentages of WO_3 were prepared by the incipient-wetness impregnation technique using aqueous ammonium meta-tungstate $(NH_4)_{10}W_{12}O_{41}{\cdot}5H_2O$ and a pre-dried homemade amorphous $ZrO_x(OH)_{4-2x}$ support[13]. The tungstated zirconia samples were dried overnight at 343 K in static air, and subsequently calcined at the desired temperature (773–1,173 K) in static air for 3 h. The following notation is used to identify the various supported tungsten oxide samples: *y*WZrOH–*T*, where *y* is the tungsten surface density (W atoms nm^{-2}), *T* is the calcination temperature (K) and ZrOH represents the amorphous zirconium oxyhydroxide support precursor.

Preparation of model supported WO_3/ZrO_2 (denoted $WZrO_2$ catalysts). Model supported $WZrO_2$ catalysts were synthesized by incipient-wetness impregnation of $(NH_4)_{10}W_{12}O_{41}{\cdot}5H_2O$ onto a crystalline ZrO_2 support (Degussa; Brunauer, Emmett and Teller (BET) surface area = 60 $m^2\,g^{-1}$)[13]. The samples were initially dried overnight under ambient conditions and subsequently calcined in flowing air at 723 K for 4 h. The following identifying notation is used: *x*$WZrO_2$–723 K, where *x* is the surface density (W atoms nm^{-2}) and ZrO_2 represents the crystalline ZrO_2 support.

The tungsten surface densities of both WZrOH and $WZrO_2$ catalysts are based on the surface area of the calcined catalyst samples. See ref. 13 for more details.

Preparation of model supported WO_3/ZrO_2 catalysts post-impregnated with additional WO_x and/or ZrO_x. Model supported WO_3/ZrO_2 catalysts co-impregnated with additional WO_x and ZrO_x were prepared by means of a two-step incipient-wetness impregnation procedure[38]. First, solutions of a desired amount of $(NH_4)_{10}W_{12}O_{41}{\cdot}5H_2O$ were impregnated onto the model supported $WZrO_2$ catalysts and dried overnight under ambient conditions. Second, a toluene solution of a desired amount of zirconium tert-butoxide, $Zr[OC(CH_3)_3]_4$, was further impregnated in a nitrogen environment in a glovebox. After the two impregnation steps, the samples were allowed to dry overnight at 293 K under nitrogen and subsequently calcined to 973 K for 4 h in flowing air. The following notation is used to describe the model WO_3/ZrO_2 catalysts co-impregnated with additional $WO_x + ZrO_x$: $(mW + nZr)/xWZrO_2$–973 K, where *m* is the surface density of the additional tungsten (in atoms nm^{-2}), *n* is the surface density of additional zirconium (in atoms nm^{-2}) and *x* is the initial surface density of WO_x on the model ZrO_2 support. It should be noted that if *m* or *n* is zero then only one of the additional components has been impregnated onto the pre-existing $WZrO_2$ catalyst.

Catalyst testing. *Methanol temperature-programmed surface reaction (TPSR) spectroscopy.* Methanol–TPSR spectroscopy was performed using an AMI-200 temperature-programmed system (Altamira Instruments) linked by a capillary tube to an online quadrupole mass spectrometer (DME200MS; Ametek Process Instruments). Methanol adsorption was performed at 373 K by flowing 2,000 ppm CH_3OH/He for 30 min. After removing residual physisorbed methanol using flowing helium at 373 K, the sample was then heated at 10 K min^{-1} to 773 K in flowing helium, and desorbed gases were analysed as a function

of catalyst temperature by mass spectrometry. Because WO_3/ZrO_2 catalysts are 100% acidic, only dimethyl ether (DME) formed and the area under the DME/CH_3OH–TPSR curve was used to calculate the number of exposed surface acid sites.

Steady-state methanol dehydration to dimethyl ether. Steady-state methanol dehydration experiments were conducted in an ambient fixed-bed quartz reactor (0.16 inch internal diameter) packed with finely ground catalyst held in place by quartz wool. A total of 5–30 mg of catalyst was used to maintain total methanol conversion below 10%, permitting the assumption of differential (that is, gradientless) reactor conditions. The catalyst samples were pre-treated for dehydration, and a reactor feed stream containing 7% CH_3OH, 14% O_2 and 79% He at 100 ml min^{-1} total flow (standard temperature and pressure, STP) was used. The reactor effluent gases were analysed using an HP5890 Series II online gas chromatograph (GC) operated in split mode for determination of methanol conversion, activity and selectivity. Steady-state performance was determined by averaging 3–4 GC cycles at 573 K. The steady-state methanol dehydration catalytic rates are expressed in terms of TOF by normalizing the reaction rate per exposed surface WO_x site per second. See ref. 13 for more details of the catalytic testing experiments.

Electron microscopy characterization. Samples for electron microscopy analysis were prepared by dipping a 300-mesh copper TEM grid, coated with a lacey carbon film, directly into the finely ground dry catalyst powder and then shaking off any loosely bound residue. HAADF images were taken on a 200 kV JEOL 2200FS (S)TEM (ref. 21) equipped with a CEOS probe C_s-corrector. Typically an ~1 Å (full-width at half-maximum, FWHM) coherent electron beam with ~30 pA probe current was used for HAADF imaging, and dwell times between 40 and 48 μs per pixel were typically applied. The HAADF images presented were low-pass filtered to reduce background noise. Chemical microanalysis by XEDS was performed on a 300 kV VG HB603 dedicated STEM (ref. 30) equipped with a Nion aberration corrector and an Oxford Instruments INCA 300 system. XEDS point analyses were carried out using an ~0.4 nm (FWHM) coherent electron beam with ~500 pA probe current.

Received 28 May 2009; accepted 1 October 2009; published online 8 November 2009

References

1. Hino, M. & Arata, K. Synthesis of solid superacid of tungsten oxide supported on zirconia and its catalytic action for reactions of butane and pentane. *J. Chem. Soc. Chem. Commun.* 1259–1260 (1988).
2. Ono, Y. A survey of the mechanism in catalytic isomerization of alkanes. *Catal. Today* **81,** 3–16 (2003).
3. Santiesteban, J. G., Vartuli, J. C., Han, S., Bastian, R. D. & Chang, C. D. Influence of the preparative method on the activity of highly acidic WO_x/ZrO_2 and the relative acid activity compared with zeolites. *J. Catal.* **168,** 431–441 (1997).
4. Scheithauer, M., Grasselli, R. K. & Knözinger, H. Genesis and structure of WO_x/ZrO_2 solid acid catalysts. *Langmuir* **14,** 3019–3029 (1998).
5. Barton, D. G., Soled, S. L., Meitzner, G. D., Fuentes, G. A. & Iglesia, E. Structural and catalytic characterization of solid acids based on zirconia modified by tungsten oxide. *J. Catal.* **181,** 57–72 (1999).
6. Barton, D. G., Shtein, M., Wilson, R. D., Soled, S. L. & Iglesia, E. Structure and electronic properties of solid acids based on tungsten oxide nanostructures. *J. Phys. Chem. B* **103,** 630–640 (1999).
7. Baertsch, C. D., Soled, S. L. & Iglesia, E. Isotopic and chemical titration of acid sites in tungsten oxide domains supported on zirconia. *J. Phys. Chem. B* **105,** 1320–1330 (2001).
8. Baertsch, C. D., Komala, K. T., Chua, Y. H. & Iglesia, E. Genesis of Brønsted acid sites during dehydration of 2-butanol on tungsten oxide catalysts. *J. Catal.* **205,** 44–57 (2002).
9. Macht, J. *et al.* Support effects on Brønsted acid site densities and alcohol dehydration turnover rates on tungsten oxide domains. *J. Catal.* **227,** 479–491 (2004).
10. Wachs, I. E., Kim, T. & Ross, E. I. Catalysis science of the solid acidity of model supported tungsten oxide catalysts. *Catal. Today* **116,** 162–168 (2006).
11. Kim, T., Burrows, A., Kiely, C. J. & Wachs, I. E. Molecular/electronic structure–surface acidity relationships of model-supported tungsten oxide catalysts. *J. Catal.* **246,** 370–381 (2007).
12. Ross-Medgaarden, E. I. & Wachs, I. E. Structural determination of bulk and surface tungsten oxides with UV–vis diffuse reflectance spectroscopy and Raman spectroscopy. *J. Phys. Chem. C* **111,** 15089–15099 (2007).
13. Ross-Medgaarden, E. I. *et al.* New insights into the nature of the acidic catalytic active sites present in ZrO_2-supported tungsten oxide catalysts. *J. Catal.* **256,** 108–125 (2008).
14. Scheithauer, M. *et al.* Characterization of WO_x/ZrO_2 by vibrational spectroscopy and *n*-pentane isomerization catalysis. *J. Catal.* **180,** 1–13 (1998).
15. Badlani, M. & Wachs, I. E. Methanol: a 'smart' chemical probe molecule. *Catal. Lett.* **75,** 137–149 (2001).
16. Barton, D. G., Soled, S. L. & Iglesia, E. Solid acid catalysts based on supported tungsten oxides. *Top. Catal.* **6,** 87–99 (1998).
17. Vartuli, J. C. *et al.* Characterization of the acid properties of tungsten/zirconia catalysts using adsorption microcalorimetry and *n*-pentane isomerization activity. *J. Catal.* **187,** 131–138 (1999).
18. Calabro, D. C., Vartuli, J. C. & Santiesteban, J. G. The characterization of tungsten-oxide-modified zirconia supports for dual functional catalysis. *Top. Catal.* **18,** 231–242 (2002).
19. Nellist, P. D. & Pennycook, S. J. Direct imaging of the atomic configuration of ultradispersed catalysts. *Science* **274,** 413–415 (1996).
20. Batson, P. E., Dellby, N. & Krivanek, O. L. Sub-angstrom resolution using aberration corrected electron optics. *Nature* **418,** 617–620 (2002).
21. Watanabe, M. *et al.* The aberration corrected JEOL JEM-2200FS FEG-STEM/TEM fitted with an Ω electron energy-filter: performance characterization and selected applications. *JEOL News* **41,** 2–7 (2006).
22. Nellist, P. D. *et al.* Direct sub-angstrom imaging of a crystal lattice. *Science* **305,** 1741 (2004).
23. Wang, S. *et al.* Dopants adsorbed as single atoms prevent degradation of catalysts. *Nature Mater.* **3,** 143–146 (2004).
24. Varela, M. *et al.* Materials characterization in the aberration-corrected scanning transmission electron microscope. *Annu. Rev. Mater. Res.* **35,** 539–569 (2005).
25. Herzing, A. A., Kiely, C. J., Carley, A. F., Landon, P. & Hutchings, G. J. Identification of active gold nanoclusters on iron oxide supports for CO oxidation. *Science* **321,** 1331–1335 (2008).
26. Borisevich, A. Y. *et al.* Dual nanoparticle/substrate control of catalytic dehydrogenation. *Adv. Mater.* **19,** 2129–2133 (2007).
27. Porcu, M., Petford-Long, A. K. & Sykes, J. M. TEM studies of Nb_2O_5 catalyst in ball-milled MgH_2 for hydrogen storage. *J. Alloys Compd.* **453,** 341–346 (2008).
28. Cortes-Jácome, M. A. *et al.* WO_x/TiO_2 catalysts via titania nanotubes for the oxidation of dibenzothiophene. *Chem. Mater.* **19,** 6605–6614 (2007).
29. Huang, X., Zhai, H. J., Li, J. & Wang, L. S. On the structure and chemical bonding of tri-tungsten oxide clusters $W_3O_n^-$ and W_3O_n ($n = 7$–10): W_3O_8 as a potential molecular model for O-deficient defect sites in tungsten oxides. *J. Phys. Chem. A* **110,** 85–92 (2006).
30. Watanabe, M. *et al.* Improvements in the X-ray analytical capabilities of a scanning transmission electron microscope by spherical-aberration correction. *Microsc. Microanal.* **12,** 515–526 (2006).
31. Varela, M. *et al.* Spectroscopic imaging of single atoms within a bulk solid. *Phys. Rev. Lett.* **92,** 095502 (2004).
32. Muller, D. A. Structure and bonding at the atomic scale by scanning transmission electron microscopy. *Nature Mater.* **8,** 263–270 (2009).
33. Yamamoto, T., Orita, A. & Tanaka, T. Structural analysis of tungsten–zirconium oxide catalyst by W K-edge and L_1-edge XAFS. *X-Ray Spectrom.* **37,** 226–231 (2008).
34. Valigi, M. *et al.* WO_x/ZrO_2 catalysts part 1. Preparation, bulk and surface characterization. *Appl. Catal. A—General* **231,** 159–172 (2002).
35. Chang, L. L. Y., Scroger, M. G. & Phillips, B. Condensed phase relations in the systems ZrO_2–WO_2–WO_3 and HfO_2–WO_2–WO_3. *J. Am. Ceram. Soc.* **50,** 212–216 (1967).
36. Klenov, D. O. & Stemmer, S. Contributions to the contrast in experimental high-angle annular dark-field images. *Ultramicroscopy* **106,** 889–901 (2006).
37. Neurock, M. Perspectives on the first principles elucidation and the design of active sites. *J. Catal.* **216,** 73–88 (2003).
38. Ross-Medgaarden, E. I. *Tuning the Electronic and Molecular Structures of Catalytic Active Sites with Oxide Nanodomains* (Lehigh University, 2007).

Acknowledgements

This work was supported by the National Science Foundation's Nanoscale Interdisciplinary Research Team (NSF-NIRT) program under grant no. 0609018. Two of the authors (M.S.W. and W.V.K.) acknowledge additional support from SABIC Americas.

Author contributions

W.Z. devised and carried out the electron microscopy experiments. E.I.R. carried out catalytic performance measurements and prepared the post-impregnation catalyst samples. W.V.K. and M.S.W. prepared some of the catalyst materials. C.J.K. and I.E.W. supervised the project. W.Z. and C.J.K. wrote the paper.

Additional information

Supplementary information accompanies this paper at www.nature.com/naturechemistry. Reprints and permission information is available online at http://npg.nature.com/reprintsandpermissions/. Correspondence and requests for materials should be addressed to C.J.K.